Obtaining glasses in the extremely crystallizing Ge–Sb–Te phase change material

A. Piarristeguy, M. Micoulaut, R. Escalier, G. Silly, M.-V. Coulet, Annie Pradel

Contents lists available at ScienceDirect

Journal of Non-Crystalline Solids

journal homepage: www.elsevier.com/locate/jnoncrysol

Obtaining glasses in the extremely crystallizing Ge–Sb–Te phase change material

A. Piarristeguy [*,a], M. Micoulaut [b], R. Escalier [a], G. Silly [a], M.-V. Coulet [c], A. Pradel [a]

[a] ICGM, Univ Montpellier, CNRS, ENSCM, Montpellier, France
[b] Sorbonne Université, Laboratoire de Physique Théorique de la Matière Condensée, CNRS UMR 7600, 4 Place Jussieu, 75252 Paris Cedex 05, France
[c] Aix-Marseille Université, CNRS, MADIREL UMR 7246, Campus de Saint Jérôme, 13397 Marseille Cedex 20, France

A B S T R A C T

Using thermal co-evaporation techniques, we show that various glassy compositions can be obtained along the $Ge_xSb_xTe_{100-2x}$ join in the ternary Ge–Sb–Te system which is known to display dramatic crystallization tendencies. Earlier attempts to produce bulk glasses have been limited to Sb-poor compositions close to the eutectic $GeTe_6$. Results indicate a weak variation of T_g with composition x and also a thermal stability that is weak for most systems, and especially for compositions close to the domain where $Ge_2Sb_2Te_5$ can be formed. Our results are put in perspective with other network-forming chalcogenides and the T_g variation suggests the preferential formation of Te–Sb–Te, at variance with isochemical compounds such as Ge–Sb–Se. Data are discussed within the framework of topological based approaches which not only indicate that optimal glass formation is achieved for compositions satisfying the Maxwell stability criterion but also predict a flexible to rigid transition at $x = 8.5\%$. Most of our glasses could be formed around this composition.

1. Introduction

Amorphous telluride thin films are now present as starting material in many electronic devices and setups, and found huge applications in the phase change (PC) memory industry [1,2]. In order to design new material functionalities for other future applications such as improved infrared transmitting waveguides or stable phase change data storage, there is a demanding need to understand in more detail the underlying factors which control the glass-forming tendency of tellurides and the relationship between structure and functional properties. In contrast with light chalcogenides (selenium and sulphide) however [3], tellurides do not form easily bulk glasses due, in part, to a high crystallization tendency and a difference in chemical bonding so that their glass-forming region (GFR) is substantially reduced as compared to corresponding selenides and sulphides. In fact, in contrast with the latter which show a weak bonding between Se/S chains, there is indeed an increased interchain cohesion in tellurium coming from a delocalized p bonding [4] so that tellurides often do not fulfill the 8-$\mathcal{N}$ rule, $\mathcal{N}$ being the number of outer shell electrons.

The halogenation of tellurides has shown to reduce crystalline nucleation by reducing Te chain lengths and the number of free electrons [5]. This has led to an extended investigation of the so-called TeX glasses (TeCl, TeI, etc.) which display increased glass-forming tendency but are also weakly connected [6]. More recently, it has been shown that a combination of Gallium and Germanium could lead to larger glass-forming regions [7,8].

One of the challenges remains still the development of Te-glasses resistant to crystallization. An interesting means in this context is to avoid the standard melt quench strategy and to search for alternative methods of glass synthesis. Recently, the deposition of Ge–Ga–Te films by thermal co-evaporation has permitted [9,10] to obtain very thick films (with thicknesses up to 17 μm) with very well controlled compositions over an increased GFR compared to the one obtained for corresponding bulk materials [11]. Similarly, the amorphous domain of the Ge–Te system could be extended not only by using thermal co-evaporation but also by employing a twin roller quenching method [12,13]. In both methods, higher quenching rates ($\simeq 10^6$ K/s) are applied as compared to that used in classical melt quenching methods to prevent from crystallization. As a result, in the Ge–Te binary glasses could be formed from 10% up to 45% Ge and glass transition temperatures T_g as well as crystallization temperatures were measured from differential scanning calorimetry experiments, together with a structural characterization [13,14].

Among chalcogenide ternary systems, the Ge–Sb–Te displays probably one of the smallest GFR (Fig. 1) that is limited to Sb-poor compositions close to the eutectic $GeTe_6$ where bulk glasses can be formed [15–20]. This is due, in part, to the large fragilities which are characteristic of liquids having small viscosities even in the deep supercooled state so that activation barriers for crystallization are low.

In the present contribution, we follow the path previously followed

* Corresponding author.

https://doi.org/10.1016/j.jnoncrysol.2021.120730
Received 20 December 2020; Received in revised form 5 February 2021; Accepted 6 February 2021

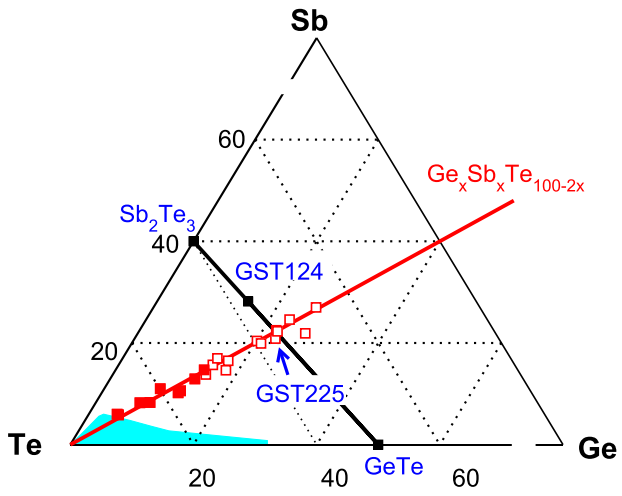

Fig. 1. Glass-forming region in the Ge–Sb–Te system (light blue zone, Katsuyama and Matsumura [15], Wei et al. [16], Lebaudy et al. [17], Fritzche and Ovshinsky [18], Dargan et al. [19], Iglason [20]). In Ge–Sb–Te, the present obtained compositions (open boxes) are found on the red line $Ge_xSb_xTe_{100-2x}$. The filled boxes indicate samples for which it was possible to measure a glass transition temperature. The typical PC materials are given in blue and are found on the Sb_2Te_3-GeTe join ($Ge_2Sb_2Te_5$ (GST225) and $Ge_1Sb_2Te_4$ (GST124)). (For interpretation of the references to color in this figure legend, the reader is referred to the web version of this article.)

for Ge-Te [12] and Ge–Ga–Te [10] and investigate the possibility to form glassy Ge–Sb–Te using thermal co-evaporation techniques. We explore the $Ge_xSb_xTe_{100-2x}$ join (red line in Fig. 1) which adds equivalently Ge and Sb atoms into the base Te network, in contrast with previous investigations targeting compositions close to the binary $GeTe_6$. Results lead to the formation of twenty-one different glassy compositions in the Ge–Sb–Te system (Fig. 1) and a weak variation of T_g with composition x is obtained, underscoring specific structural features. Calorimetric glass transitions are evidenced essentially for compositions being close to the Maxwell stability criterion that has been previously used to identify optimal glasses. The thermal stability $T_x - T_g$ (T_x being the temperature of crystallization onset) is close to zero for Te- and (Ge,Sb)-rich systems, especially close to the domain where $Ge_2Sb_2Te_5$ (GST225) can be formed, and for the latter no glass transition can be obtained at the heating rate used. The present results not only extend the glass-forming range of the technologically important Ge–Sb–Te phase change material but also reveals aspects of structure which control the glass-forming ability and T_g.

2. Preparation methods

2.1. Film elaboration

The exploration of the Ge–Sb–Te system was conducted by studying twenty-one compositions close to the composition line $Ge_xSb_xTe_{100-2x}$. Films with different compositions and thicknesses (ranging from 3 to 9 μm) were obtained by varying the evaporation rates of the three elements Ge (Goodfellow, lump, 99.999%), Sb (Sigma-Aldrich, beads, 99.999%) and Te (Sigma-Aldrich, pieces, 99.999%) and the deposition duration. $Ge_xSb_xTe_{100-2x}$ films were deposited by thermal co-evaporation using a PLASSYS MEB 500 device equipped with two current induced heating sources and an electron beam evaporator. The three sources were placed in a configuration that allowed the deposition of films with uniform composition and thickness over a surface of about 4 cm in diameter [21]. The two current induced heated sources were used to evaporate Antimony and Tellurium, whereas the electron beam was used to evaporate Germanium. Sb and Te were placed in two homemade carbon crucibles inserted in Molybdenum nacelles covered with a perforated Molybdenum foil, in order to ensure a stable evaporation rate. Germanium was placed in the electron beam using a Copper crucible. The microscope slides used as substrates were cleaned with alcohol and dried with dry air. Before the deposition, the chamber was evacuated down to approximately 10^{-5} Pa. During the deposition process, the substrate holder was rotating at 8 rpm. The evaporation rate and thickness for each element were automatically controlled with pre-calibrated quartz crystal monitors. A typical film deposition rate of 420 nm/min was applied. Let us note that no further annealing treatment was carried out prior to proceeding to the film characterization.

2.2. Film characterization

The chemical composition of ternary $Ge_xSb_xTe_{100-2x}$ glasses was estimated by Electron Probe Micro-Analyser (EPMA) using a CAMECA SX-100 instrument with an acceleration voltage of 20 kV and a probe current of 10 nA. Table 1 displays the comparison between targeted compositions and the measured compositions.

The amorphous nature of the film was checked by X-ray diffraction (DRX) using a Panalytical XPERT diffractometer. A Cu (Kα) source (λ = 1.5406 Å) was used for the excitation with operating voltage of 40 kV with a beam current around 30–40 mA. The X-ray diffractograms of all deposited films, whatever their thickness, showed broad peaks indicating an amorphous structure (Fig. 2).

The thermal behavior of eight glass compositions close to the $Ge_xSb_xTe_{100-2x}$ line was investigated by Differential Scanning Calorimetry (DSC) using a METTLER DSC30 (Table 1). The thicknesses of the films being around 3 μm, it was possible to study their thermal behavior using calorimetry. Around 8–10 mg of sample were put into Aluminum

Table 1
Targeted compositions and EPMA analyzed compositions for the DSC study with measurements of the glass transition temperature (T_g), the temperature of crystallization onset (T_x) and the crystallization temperatures (T_{c1}, T_{c2}, T_{c3}) (in °C).

Measured composition	Targeted composition	T_g (°C) ±2 °C	T_x (°C) ±2 °C	T_{c1} (°C) ±0.5 °C	T_{c2} (°C) ±0.5 °C	T_{c3} (°C) ±0.5 °C
$Ge_{4.6}Sb_{6.0}Te_{89.4}$	$Ge_{5.3}Sb_{5.3}Te_{89.4}$	81	86	104.0		
$Ge_{8.8}Sb_{8.3}Te_{82.9}$	$Ge_{8.6}Sb_{8.6}Te_{82.8}$	99	111	130.6		
$Ge_{9.1}Sb_{11.0}Te_{79.9}$	$Ge_{10}Sb_{10}Te_{80}$	104	113	131.5		
$Ge_{12.4}Sb_{10.2}Te_{77.4}$	$Ge_{11.3}Sb_{11.3}Te_{77.4}$	114	132	150.9	161.1	297.5
$Ge_{14.4}Sb_{14.7}Te_{70.9}$	$Ge_{14.5}Sb_{14.5}Te_{71}$	124	133	149.1	165.6	
$Ge_{17.4}Sb_{16.5}Te_{66.2}$	$Ge_{17}Sb_{17}Te_{66}$		134	153.2	176.2	
$Ge_{20.5}Sb_{20.4}Te_{59.1}$	$Ge_{20.5}Sb_{20.5}Te_{59}$		129	141.2	179.7	224.2
$Ge_{23.3}Sb_{24.6}Te_{52.2}$	$Ge_{23.9}Sb_{23.9}Te_{52.2}$ (≃ GST225)		118	136.4		

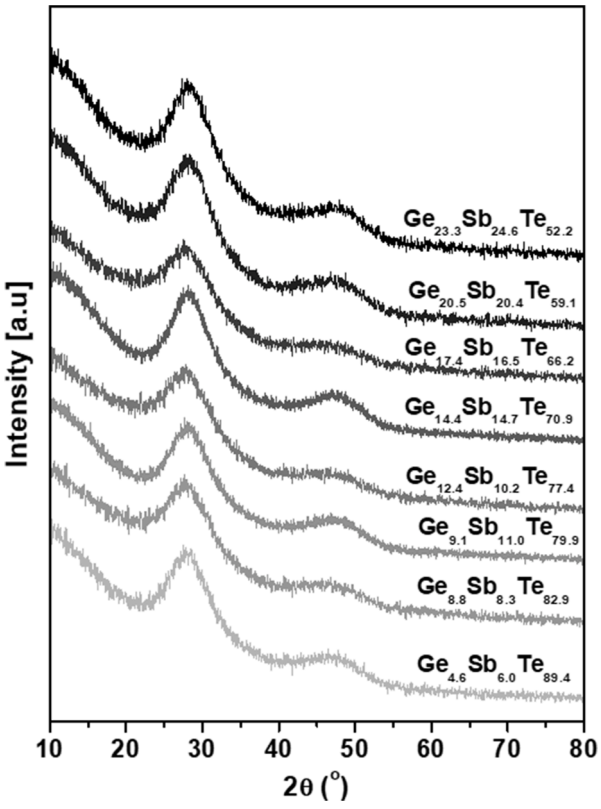

Fig. 2. Diffractograms of the various investigated compositions.

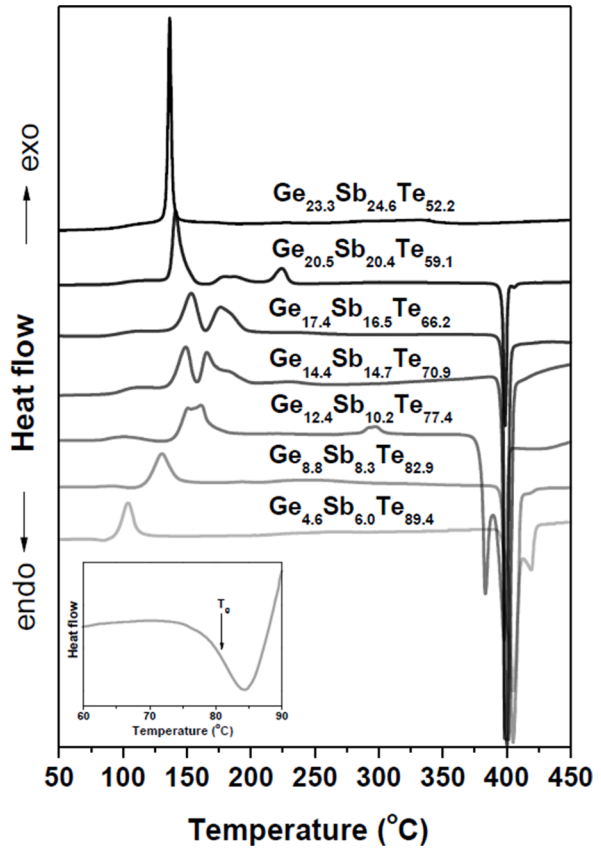

Fig. 3. Typical DSC scans of Ge–Sb–Te glasses obtained by thermal co-evaporation techniques. The inset shows the DSC signature of a typical glass transition (here $Ge_{4.6}Sb_{6.0}Te_{89.4}$).

pans. The container was afterward hermetically closed under atmosphere. The experiments were performed under Argon flux with a continuous heating rate of 10 °C/min from room temperature up to 500 °C.

The powders used for DRX and DSC measurements were obtained by scraping the previously deposited films.

The transmission spectra of the thick films were recorded between 800 and 2500 nm using a CARY5000 spectrophotometer from VARIAN. They were used to determine the optical band gap E_g for the different compositions, thanks to the Tauc's method [22].

3. Results

As represented in Fig. 3, the DSC curves obtained for Ge–Sb–Te films with $4.6\% \leq x \leq 23.3\%$ Ge show i) a change in the baseline related to the change in specific heat at the glass transition, ii) at least one exothermic peak due to the crystallization and iii) an endothermic peak linked with the melting of the structure. The characteristics temperatures of the various transitions are given in Table 1.

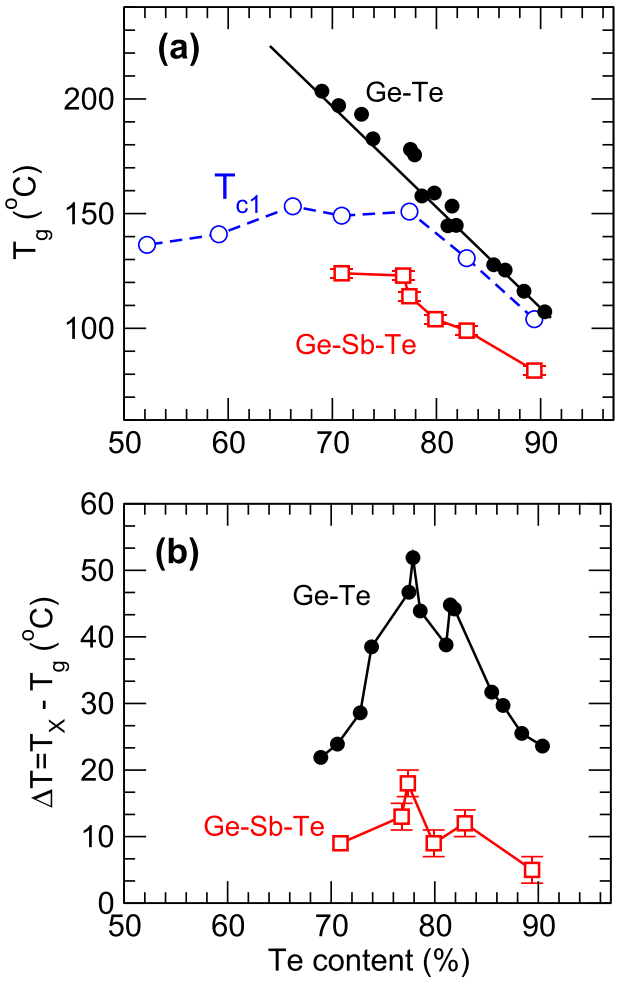

Fig. 4. (a) Evolution of the glass transition temperature T_g with Te content in $Ge_xSb_xTe_{100-2x}$ glasses (red squares), compared to corresponding measurements in Ge_xTe_{100-x} [14]. The black line in Ge–Te is a parameter-free predication from SAT [28]. The blue dotted line corresponds to T_{c1}. (b) Thermal stability $\Delta T = T_X - T_g$ for both systems. (For interpretation of the references to color in this figure legend, the reader is referred to the web version of this article.)

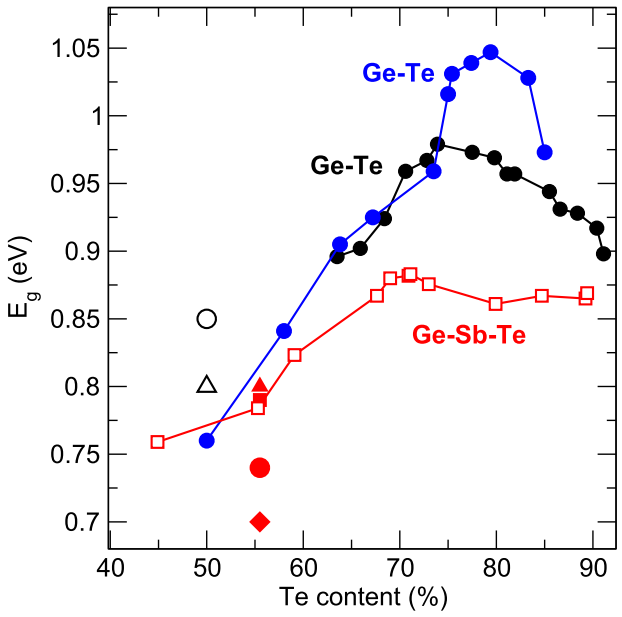

Fig. 5. Optical gap E_g measured in the present Ge–Sb–Te (red filled boxes), and compared to similar results for Ge-Te (black [29] and blue filled circles [30]). Independent results are given for GeTe (black open box [31], triangle [32]) and GST225 (red open box [31], triangle [32], diamond [33], circle [34]). (For interpretation of the references to color in this figure legend, the reader is referred to the web version of this article.)

3.1. Glass transition

From the available data, one can observe that, between ≃ 70.9 and 89.4 at.% Te, the glass transition temperature T_g decreases while the Te content increases. This trend is similar to the one obtained for a parent system (binary Ge_xTe_{100-x}) in which T_g steadily increases with x (Fig. 4a), whereas the crystallization temperature T_x, defined as the onset temperature of the first exothermic peak, is maximum for the compositions with intermediate Te content (≃66–74%) and lower for the Te-rich and Te-poor compositions.

To determine the stability of the glass, we calculate the difference ΔT between T_x and the glass transition temperature T_g (Fig. 4b). It is generally admitted that a good glass former displays a difference of $\Delta T \geq 100$°C. As detected from both Table 1 and Fig. 4b, for the present Ge–Sb–Te glasses, this difference is always lower than 20 °C, and this clearly indicates the strong tendency to crystallize at those compositions. This tendency also observed in GeTe glasses, is stronger in the GeSbTe system, probably because of the presence of Sb, kwown to easily crystallize close to room temperature [23].

Interestingly, the crystallization process depends dramatically on the tellurium content and can be single step, two-steps or even three steps which suggests that depending on the composition, the crystallization leads to different phases underscoring the complexity of the Ge–Sb–Te phase diagram [24], and might be initiated even in the glassy state, as crystallization kinetics appears to be present even in the glassy state [25, 26].

With increasing Ge/Sb content, T_g and T_{c1} first increase up to 124 °C and 153.2 °C, respectively, up to approximately x ≃14–17% (Fig. 4). Once x is further increased, glass transition temperatures are barely measurable. The limit in Te-concentration of amorphous samples displaying a T_g is found to be close (70.9%) to the one found for the parent Ge–Te system obtained with the same co-evaporation technique (67%, Jóvári et al. [13], Piarristeguy et al. [14]). It is also important to recognize the absence of a calorimetric signature of T_g in the PC region (i.e. GST225) at the used heating rate.

At low modification, the T_g values are very close to those obtained for the parent Ge–Te system [14] and a linear fit down to elemental Te ($x = 0$) yields $T_g(0) = 58.5(8)$°C for Ge–Te and 58.4(6)°C for Ge–Sb–Te, i.e. rather close to a previous reported value of amorphous Te [27]. In the Te-rich domain, the T_g linear variation furthermore reflects the random addition of Ge/Sb atoms in the structure that can be predicted using stochastic agglomeration theory (SAT, Micoulaut [28]) which displays a parameter-free slope equal to :

$$\left[\frac{dT_g(x)}{dx}\right]_{x=0} = \frac{T_g(0)}{\ln 2} \quad (1)$$

3.2. Crystallization temperature

As mentioned above, for select compositions the shape of the crystallization peak (Fig. 3) indicates the coexistence of at least two separate

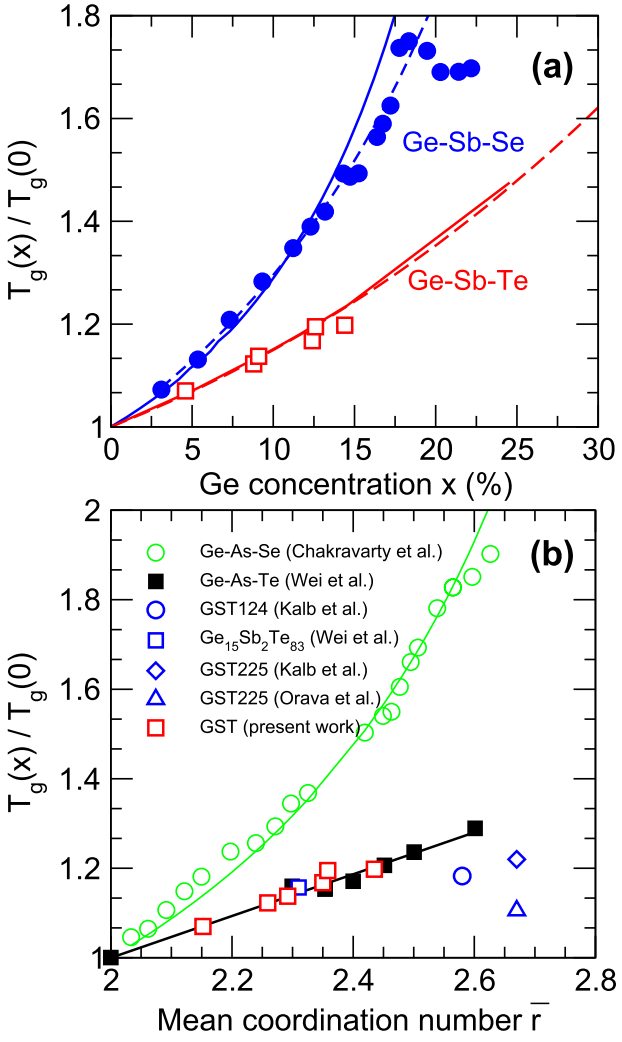

Fig. 6. (a) Ratio $T_g(x)/T_g(0)$ as a function of x in Ge–Sb–Se [40] and Ge–Sb–Te (present results) with $T_g(0) = 316$ K for Se system and the determined $T_g(0) = 58.4$ °C = 331.8 K for Te system. Note that x represents here the Ge content. The blue solid line is a prediction from SAT assuming coordinations $r_{Sb} = 3$ and $r_{Ge} = 4$ [39], whereas the broken blue line is a GDM fit with $\beta = 0.76$. The solid red curve is also a GDM fit but with $\beta = 0.44$, and the broken red line corresponds to a SAT prediction assuming the preferential formation of Sb_2Te_3. (b) Compilation of data represented as a function of mean coordination number $\bar{r}$: Ge–As–Se [40], Ge–As–Te [16], GST124 [42], $Ge_{15}Sb_2Te_{83}$ [16], GST225 [42, 43]). For the GST systems, compositions in Table 1 have been used. The green curve is a GDM fit [44] with $\beta = 0.80$. (For interpretation of the references to color in this figure legend, the reader is referred to the web version of this article.)

crystalline phases in the sample (e.g. for $Ge_{17.4}Sb_{16.5}Te_{66.2}$). The DSC signals exhibit, indeed, several strong exothermic peaks at different crystallization temperatures T_{ck} ($k = 1,2,3$), the number of such events being dependent on the considered composition (Fig. 3). We note that for Te-rich glasses, there is only a single peak at e.g. 104 °C for $Ge_{4.6}Sb_{6.0}Te_{89.4}$ and the same prevails for compositions close to GST225, with a peak at 136.4°C for $Ge_{23.3}Sb_{24.6}Te_{52.2}$ (Table 1).

3.3. Optical band gap

Fig. 5 represents the behavior of the optical gap E_g in Ge–Sb–Te glasses as a function of the Ge/Sb content. When compared to Ge–Te, it is found that $E_g(x)$ displays a similar trend with increasing Ge/Sb concentration, i.e. starting from a gap $E_g \simeq 0.85$ eV for pure Te (compatible with 0.90 eV, [35]), the gap slightly increases and passes a maximum at about 15% Ge, prior to an important decrease that is also acknowledged in the corresponding Ge–Te glasses [29,30]. The gap measured in the PC region for GST225 is consistent with other experimental measurements [31–34]. Note that in the Te-poor region data of Ge_xTe_{100-x} and $Ge_xSb_xTe_{100-2x}$ nearly coalesce on a single line with a similar slope $dE_g(x)/dx \simeq 0.07$, which indicates that E_g is essentially driven by the reduction of the presence of Te atoms.

4. Discussion

Based on our measurements, we are now able to state that the GFR of Ge–Sb–Te is larger than previously believed, and our results extend the previously reported Sb-poor domain close to the *GeTe*$_6$ eutectic [15–20] to compositions containing an equivalent amount of Ge and Sb atoms. Previous co-evaporation investigations have also led to an extension of GFR as in Ge-Te [12] or Ge–Ga–Te [10], and the technique appears, therefore, as a promising tool for the generation of amorphous alloys prone to crystallization. It is known that glass-forming ability is increased close to eutectics which bring the supercooled liquid to lower temperatures and higher viscosities, the latter acting as barriers against crystallization [36]. It is interesting to note from the Te-$Ge_2Sb_2Te_5$ isopleth which corresponds exactly to our $Ge_xSb_xTe_{100-2x}$ join, that a freezing-point depression (i.e. eutectic-like transformation) does exist for $x \simeq 7.5\%$, and it extends the liquid phase down to 406 °C [24]. Based on this observation, one can reasonably argue that an optimal glass formation can be expected around the $Ge_{7.5}Sb_{7.5}Te_{85}$ composition.

It is insightful to compare the obtained glass transition temperatures T_g with respect to chemical analogues or parent systems. The isocoordination rule signals [37,38], indeed, that for a variety of chalcogenide glasses, physico-chemical properties essentially depend on the network topology that is characterized by the average coordination number or connectivity:

$$\bar{r} = \sum_k r_k x_k \tag{2}$$

where r_k is the coordination of species k with concentration x_k. For ternary chalcogenides studied along the present compositional join and involving atoms of Group IV and V, at a first approximation this average coordination number, thus, should behave as $\bar{r} = 2(1 - 2x) + 4x + 3x = 2 + 3x$ ($r_{Ge} = 4$, $r_{Sb} = 3$ and $r_{Te} = 2$). As a result, one might expect that the glass transition temperature in e.g. Ge–Sb–Se, Ge–Sb–Te or Ge–As–Te should behave rather similarly as it is the case when binary chalcogenides are represented as a function of the single quantity $\bar{r}$ [28,39].

4.1. Learning from T_g variation

Fig. 6 a represents the glass transition temperature variation of two *a priori* similar systems, i.e. $Ge_xSb_xSe_{100-2x}$ [40] and the present $Ge_xSb_xTe_{100-2x}$ one. Results clearly indicate a radically different behavior encoded in the way the initial chalcogen chain network is altered by (Ge,Sb) atomic crosslinks, an observation that can be also made for Ge-As-X (X = Se,Te) glasses [16,40] (panel b). Here, T_g is given as a function of $\bar{r}$ (Eq. (2)) in order to represent on the same plot sets of data accumulated from different compositional joins in the ternary phase diagram, and for all, it was chosen $r_{Ge} = 4$, $r_{Sb} = 3$ and $r_{Te} = 2$. While this is of course partially valid in tellurides, alternative coordination numbers (i.e. $r_{Sb} > 3$ and $r_{Te} > 2$ [41]) do not afffect the conclusions but are discussed below.

4.1.1. Connectivity driven T_g

For the selenide compounds, T_g can be predicted from a parameter-free equation from SAT (broken blue line, Fig. 6a, [39]) :

$$\bar{r} = 2r_B r_C \frac{2r_C\alpha^2(1-\gamma) + 2r_B\gamma^2(1-\alpha) + r_B r_C \alpha\gamma(\alpha\gamma - \alpha - \gamma)}{(2r_C\alpha + 2r_B\gamma - r_B r_C \alpha\gamma)^2 - 8r_B r_C \alpha\gamma} \tag{3}$$

where $r_B = r_{Ge} = 4$ and $r_C = r_{Sb} = 3$.

$$\alpha = \left(\frac{2}{r_C}\right)^{T_0/T_g}, \quad \gamma = \left(\frac{2}{r_B}\right)^{T_0/T_g}, \quad \delta = \left(\frac{4}{r_B r_C}\right)^{T_0/T_g} \tag{4}$$

Alternatively, it has been shown [44] that such glasses also follow a modified Gibbs Di Marzio (GDM) equation [45] initially proposed for cross-linked polymers, and which writes:

$$T_g(\bar{r}) = \frac{T_g(\bar{r} = 2)}{1 - \beta(\bar{r} - 2)} \tag{5}$$

with β a parameter that can be fitted to the data ($\beta = 0.80$ for Ge–As–Se, Fig. 6b) or calculated [46,47]. Both predictions reproduce very accurately the T_g data for the selenide compounds but the direct application of Eq. (3) to the tellurides obviously fails, and a fit of Eq. (5) to the data collection of Ge–As–Te [16] and the present Ge–Sb–Te leads to a value in the Te-rich region ($\beta = 0.44$) that is incompatible with its microscopic origin which usually leads to values close to 0.65–0.80 [46–48], unless some additional structural assumptions are tested. Different network based models of the glass transition have, indeed, shown that for chalcogens β scales e.g. [46] as :

$$\beta^{-1} = \sum_{k=1}^{N} (r_k - r_X) \ln\left[\frac{r_k}{r_X}\right] \tag{6}$$

with X = S,Se,Te and N the number of cross-linking species involved. Corresponding coordinations $r_k = 4, 3,$ and 2 for k = Ge, Sb, and Te, respectively, lead to $\beta^{-1} = \ln 2 + \ln 3$, i.e. $\beta = 0.56$ that is also rather different from the fit to the data (0.44). Coordinations determined from molecular simulations do not alter the conclusion, i.e. with $r_k = 3.85$, 3.12 and 1.99 for k = Ge, Sb, and Te [41], one obtains $\beta \simeq 0.57$. The trend in T_g in Ge–Sb–Te must be driven from some other microscopic alteration of the base Te network.

4.1.2. Signature of preferential bonding

Given the trend in T_g, it appears more likely that these Ge–Sb–Te display a tendency towards preferential bonding and eventually nanoscale phase separation possibly induced by the rather stressed rigid nature of their network structure [14]. This feature has been also determined in e.g. Ge–Se glasses [49], and usually manifests by a maximum in T_g as e.g. detected at $x \simeq 17\%$ in Ge–Sb–Se (Fig. 6a, [40]), followed by a nearly constant value of the glass transition temperature.

Our argument builds on the SAT functional forms of T_g given in Eqs. (3)–(6). Effect of chemical ordering can be taken into account by considering an amorphous network of the form $Te_{1-x-y}Ge_ySb_x$ and assuming a general tendency to form Te–Sb–Te bonds and a compound cluster of stoichiometry Sb_2Te_3 inside a Te-rich random network. This compound cluster has a constant connectivity and does not contribute to the increase in T_g [48]. Once the system is rewritten as $[Sb_2Te_3]_{x/2}Ge_yTe_{1-5x/2-y}$, this defines an effective concentration y_{eff} for

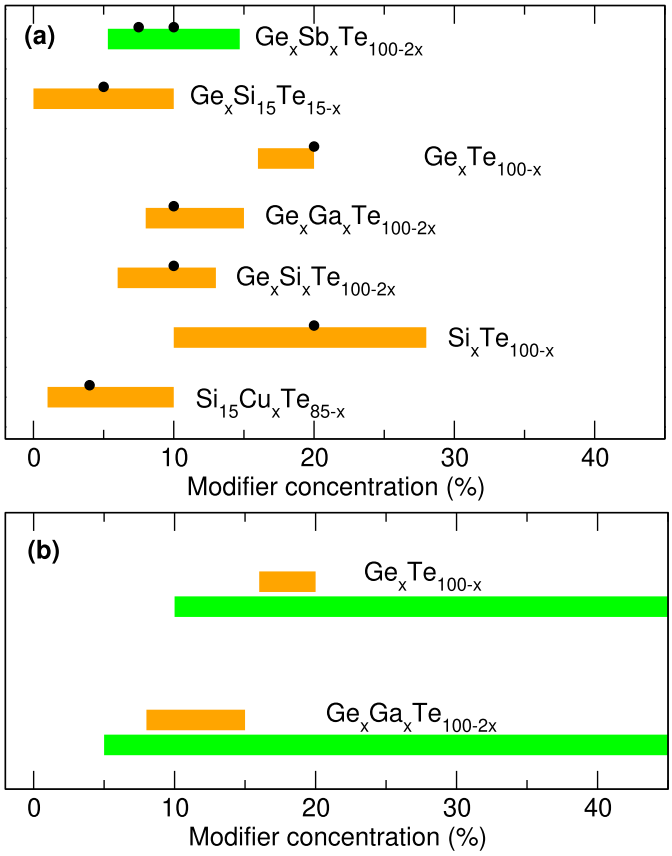

Fig. 7. (a) GFR (bars) and *locus* of the flexible-rigid transition satisfying the Maxwell stability criterion $n_c = 3$ (filled circles) for various telluride glasses reported in the literature: $Ge_xSb_xTe_{100-2x}$ (present work) compared to melt-quenched $Ge_xSi_{15}Te_{85-x}$ [74,75], $Ge_xGa_xTe_{100-2x}$ [6], $Ge_xSi_xTe_{100-2x}$ [70], Si_xTe_{100-x} [76], $Si_{15}Cu_xTe_{85-x}$ [77]. The GFR of the present Ge–Sb–Te corresponds to the filled squares in Fig. 1. (b) GFR of melt-quenched (orange, same as panel a) and co-evaporated samples (green): Ge_xTe_{100-x} [14] and $Ge_xGa_xTe_{100-2x}$ [9,10]. (For interpretation of the references to color in this figure legend, the reader is referred to the web version of this article.)

the Ge atoms in the glassy matrix given by:

$$y_{eff} = \frac{y}{1 - \frac{5x}{2}} \tag{7}$$

and a corresponding average coordination number of :

$$\bar{r} = r_{Te} + \frac{(r_{Ge} - r_{Te})y}{1 - \frac{5x}{2}} \tag{8}$$

Using Eq. (7) with $x = y$ and in combination with (3), we can now represent the predicted glass transition temperature variation $T_g(x)$ in the case where a preferential formation of Sb_2Te_3 is assumed (broken red line in Fig. 6). Using $r_{Ge} = 4$ and $r_{Te} = 2$, results now agree with the measured T_g data up to the limit of the present glass-forming range ($0 \leq x \leq 15\%$), where it should be also noted that a moderate change in coordination numbers (see above) does not alter the tendency drawn by the equations derived from SAT. The present Ge–Sb–Te systems, thus, clearly departs from its selenide analogue.

4.1.3. Nanoscale phase separation

In Ge–Sb–Se, a maximum in T_g is obtained at $x \simeq 17\%$ (Fig. 6a). This anomaly is usually linked with the onset of a nanoscale phase also characterized from spectroscopic probes [50,51] which signals the occurence of homopolar Ge–Ge and Sb–Sb bonds and the emergence of Ge ethane- and Sb ethylene-like units for $x \geq 17\%$. The loss in global connectivity of the glass network upon nucleation of these Ge and Sb-rich nanophases leads to a reduction of the T_g increase with connectivity [50], a maximum and a near constant value of the glass transition temperature for larger x [40,49]. Once different data are collected from the PC region [16,42,43], the near constant value of T_g with composition for $\bar{r} \geq 2.45$ (Fig. 6b) also signals the reduction in connectivity that might arise from such nanoscale phase tendencies which have been detected in the related binary Ge–Te [14], and have also been suggested from connectivity arguments [52].

Related binary Sb chalcogenides display strong tendencies to phase separation and crystallization of the melts. In selenides Sb_xSe_{100-x}, a decoupling into a Se-rich phase and a stoichiometric-like Sb_2Se_3 phase is observed [53] and this extends within compositions belonging to an immiscibility dome over $5 \leq x \leq 35\%$ Sb [54]. As a result, T_g of such glasses remains constant for $x \geq 5\%$ and display a plateau behavior [55]. For the Sb–Te tellurides, we are not aware of any glass forming range and this system appears to be subject to important crystallization tendencies.

4.2. The special case of GST225

There have been a certain interest in determining T_g of the prototypal phase change material $Ge_2Sb_2Te_5$ given its use in crystalline-amorphous transition for applications in data storage. Different measurements apparently lead to a spread in reported values ranging from 100 °C to 200 °C. Using a variety of probes (DSC but also impedance and optical transmission measurements [56]), Morales–Sanchez found for sputtered films $T_g = 100$ °C, whereas Kalb et al. determined T_g at some higher value (182 °C) from the lower bound of evaluated viscosities [57], or from DSC on pre-annealed samples [42]. Additional studies have also confirmed the temperature range where the glass transition occurs in GST225, the determined values being largely dependent on measurement method and sample preparation which relies mostly magnetron sputter deposition from stoichiometric targets [43,58–60], the spread in T_g measurements being possibly influenced by the film thicknesses which is known to influence T_g [61].

Our DSC measurement on the composition that is the closest to GST225 ($Ge_{23.3}Sb_{24.6}Te_{52.2}$) indicates absence of a calorimetric T_g (Table 1). We interpret such an absence from the applied scan rate of 10 °C/min which is too slow to avoid the rapid crystallization above T_g. Recent ultrafast DSC experiments have, indeed, indicated that an endotherm related to T_g starts to be visible in GST225 for scan rates larger than 40 K/min [25].

4.3. Glass formation and rigidity transitions

In the rigidity picture of Phillips [62] and Thorpe [63], an amorphous network can be seen as a mechanical truss where the nodes (i.e. the atoms) are constrained by bending and stretching interactions. This network is rigid but stress-free when the density of such topological constraints n_c equals 3. The system is then at a mechanical critical point defining a flexible to rigid transition that influences the glass-forming ability, and which lead to a nearly vanishing of the relaxation enthalpy at the glass transition [64]. In fact, the number of internal degrees of freedom (i.e. flexible modes) nearly vanishes at $n_c = 3$, and decreases the corresponding relaxation in the potential energy landscape that would bring an additional increase to the heat of vitrification [65]. Conversely, the absence of excess constraints/stress prevents from phase separation which manifests only at the limit of the GFR for glasses having a large cross-link density [40,50]. Glass formation at the rigidity transition composition $n_c = 3$ is therefore identified as optimal, and different authors have reported signatures of the enhanced ability to form glasses [66,67].

While the notion of covalency which is central to the rigidity approach may not be fully valid in tellurides due to the increased

metallic character and the partial loss of covalent bonding, recent algorithms have permitted to enumerate topological constraints from classical or ab initio molecular dynamics simulations [68], the latter permitting to treat exactly the chemical bonding within density functional theory. Also, experiments have indicated that the usual anomalies found in e.g. selenides are also observed in tellurides [69–71] but with a probable failure of the isocoordination rule and an obvious breakdown of the 8-$\mathcal{N}$ (octet) rule as e.g. Gallium has a coordination of four in Te-based glasses [12].

An application of such algorithms on density functional based models of select Ge–Sb–Te compositions has led to the recognition of a flexible to rigid transition (i.e. a Maxwell stability line) close to the compositional join $GeTe_4-SbTe_4$ or to the $GeSbTe_8$ compound ($x_c \simeq 10\%$) on the present $Ge_xSb_xTe_{100-2x}$ line [72]. A more recent and systematic analysis using such tools but in an improved fashion gives a similar result ($x_c \simeq 8.5\%$, [73]).

It is interesting to note that $Ge_xSb_xTe_{100-2x}$ glasses obtained by coevaporation are found from either side of the locus x_c of the rigidity transition defining optimal glasses according to Phillips [62]. A perusal of the GFR of different melt-quenched telluride glasses (Fig. 7a) shows that this correlation holds for different telluride systems involving e.g. Group IV and V elements. While some of these GFR are reduced with respect to their selenide or sulfide counterparts, previous use of coevaporation on amorphous tellurides have demonstrated that the GFR can be extended with respect to ordinary melt-quenched composition [9,10] as in Ge–Te or Ge–Ga–Te (Fig. 7b).

In Ref. [30], it was argued that for Ge_xTe_{100-x} a Maxwell stability line and an underlying flexible to stressed transition could be detected from conductivity measurements as stressed rigid glasses ($x > x_c = 26.5\%$) exhibit rather strong resistance drift with time. The transition manifests also in the optical band gap $E_g(x)$ which displays a maximum at x_c (Fig. 5) and drives the anomalous conductivity behavior of the amorphous phase, and also the ageing behavior [29]. In the present Ge–Sb–Te, while the maximum is less evident than for Ge–Te, a clear change in regime is found at $x \simeq 15\%$ as E_g decreases substantially for larger compositions.

5. Conclusion

Amorphous $Ge_xSb_xTe_{100-2x}$ thick films have been deposited by co-thermal evaporation and have permitted to extend for the first time the glass-forming domain in the Ge–Sb–Te ternary, a system which is known to be prone to enhanced crystallization tendencies. Previous investigations were, indeed, limited to Sb poor compositions close to the $GeTe_6$ eutectic. Here, glasses with thicknesses as large as 9 μm could be formed over a wide range of composition between 52.2% and 89.4% Te. DSC experiments have revealed that the stability of the glasses against crystallization decreases with increasing the Te content, and for select compositions a multi-step crystallization process has been observed which is related to the complex phase diagram of Ge–Sb–Te and the crystallization of stoichiometric distinct phases within a reduced temperature interval.

The analysis of the $T_g(x)$ variation and its comparison with parent systems (Ge–Sb–Se, Ge–As–Te,...) reveals profound differences but also similarities. The effect of network connectivity as well as the tendency to form select preferential bonding Te–Sb–Te has been analyzed within the framework of stochastic agglomeration theory that permits to predict T_g with x or $\bar{r}$. Finally, using the salient observations, features and results valid in Se- and S-based glasses, we acknowledge the possible link between the GFR and a flexible to rigid transition close to $Ge_{10}Sb_{10}Te_{80}$ [72,73]. Along the targeted join in the Ge–Sb–Te diagram, a calorimetric T_g can be measured in this GFR which ends at $x \simeq 15\%$ so that the PC region close to GST225 is characterized by a rapid recrystallization which overwhelms the glass transition signature that cannot be detected using our DSC scan rate.

On the overall, these results clearly reveal an increased complexity of the diagram of amorphous Ge–Sb–Te and the possibility to produce glasses far away from the $GeTe_6$ eutectic, and with a balanced amount of Ge and Sb atoms. As a final comment we stress that the Ge–Sb–Te GFR initially represented in Fig. 1 obviously needs a serious update. Open questions remain such as (i) the possibility to form melt-quenched glasses on the $Ge_xSb_xTe_{100-2x}$ join, (ii) the nature of the underlying dynamic behavior encoded in e.g. the fragility evolution of the corresponding supercooled melts, and (iii) the direct link with flexible-rigid transition and intermediate phases which are generic to chalcogenides.

Declaration of Competing Interest

The authors declare that they have no known competing financial interests or personal relationships that could have appeared to influence the work reported in this paper.

Acknowledgments

The work was carried out in the framework of the Project ANR-2011-BS08-012-01 (project TEAM). A.P., R.E. and A.P. acknowledge Claude Merlet and Joël Couve for their help in EPMA and DSC experiments, respectively.

References

[1] W. Zhang, R. Mazzarello, M. Wuttig, E. Ma, Nat. Rev. Mater. 4 (2019) 150.
[2] S. Raoux, M. Wuttig (Eds.), Phase Change Materials and Applications, Springer, Berlin, 2008.
[3] A.V. Kolobov, K. Shimakawa (Eds.), Amorphous Chalcogenides: Structure, Properties, Modeling and Applications. World Scientific, 2020.
[4] J. Akola, R.O. Jones, S. Kohara, T. Usuki, E. Bychkov, Phys. Rev. B 81 (2010) 094202.
[5] J. Lucas, X.H. Zhang, J. Non-Cryst. Solids 125 (1990) 1.
[6] S. Danto, P. Houizot, C. Boussard-Pledel, X.H. Zhang, F. Smektala, J. Lucas, Adv. Funct. Mater. 16 (2006) 1847.
[7] P. Petkov, V. Ilchev, T. Petkov, P. Ilchev, AIP Proc, 2010, 1203, 932.
[8] B. Bureau, C. Boussard-Pledel, P. Lucas, X. Zhang, J. Lucas, Molecules, 2010, 14, 4337.
[9] I. Pethes, A. Piarristeguy, A. Pradel, S. Michalik, R. Nemausat, J. Darpentigny, P. Jóvári, 2020, J. Alloy. Compd., 834, 155097.
[10] J. Frayret, E. Barthelemy, S. Albert, C. Vigreux, A. Pradel, Optoelectron. Adv. Mater. Rapid Commun., 2009, 3(3), 260.
[11] S. Danto, P. Houizot, C. Boussard-Pledel, X.H. Zhang, F. Smektala, J. Lucas, Adv. Funct. Mater. 16 (2006) 1847.
[12] A.A. Piarristeguy, E. Barthélémy, M. Krbal, J. Frayret, C. Vigreux, A. Pradel, J. Non-Cryst. Solids, 2009, 355, 2088.
[13] P. Jóvári, A. Piarristeguy, R. Escalier, I. Kaban, J. Bednarcik, A. Pradel, J. Phys. 25 (2013) 195401.
[14] A. Piarristeguy, M. Micoulaut, R. Escalier, P. Jóvári, I. Kaban, J. van Eijk, J. Luckas, S. Ravindren, P. Boolchand, A. Pradel, J. Chem. Phys. 143 (2015) 074502.
[15] T. Katsuyama, H. Matsumura, J. Non-Cryst. Solids 139 (1992) 177.
[16] S. Wei, G.J. Coleman, P. Lucas, C.A. Angell, Phys. Rev. Appl. 7 (2017) 034035.
[17] P. Lebaudy, J.M. Saiter, J. Grenet, M. Belhadji, C. Vautier, Mater. Sci. Eng. A 132 (1991) 132.
[18] H. Fritzche, S. Ovshinsky, J. Non-Cryst. Solids 2 (1970) 148.
[19] S.L. Dargan, P. Burton, S.V. Phillips, A.S. Bloor, P. Nesvaba, J. Mater. Sci. 9 (1974) 1495.
[20] M. Iglason, Solid State Commun., 1982, 44, 247.
[21] V.T. Mai, R. Escalier, C. Vigreux, A. Pradel, Thin Solid Films 524 (2012) 309.
[22] J. Tauc, R. Grigorovici, A. Vancu, Phys. Status Solidi B 15 (1966) 627.
[23] N. Kaiser, Thin Solid Films, 1984, 116, 259.
[24] B. Legendre, C. Hancheng, S. Bordas, M.T. Clavaguera-Mora, Thermochim. Acta 78 (1987) 141.
[25] R. Jeyasingh, S.W. Fong, J. Lee, Z. Li, K.-W. Chang, D. Mantegazza, M. Asheghi, K. E. Goodson, H.S.P. Wong, Nano Lett. 14 (2014) 3419.
[26] J. Pries, S. Wei, M. Wuttig, P. Lucas, Adv. Mat. 31 (2019) 1900784.
[27] D. Derewnicka, P. Zielinski, H. Davies, J. Mater. Sci. Lett., 1982, 1, 87.
[28] M. Micoulaut, Eur. Phys. J B 1 (1998) 277.
[29] A. Piarristeguy, A. Pradel, J.-Y. Raty, MRS Bull.2017, 42, 45.
[30] J. Luckas, A. Olk, P. Jost, H. Volker, J. Alvarez, A. Jaffré, P. Zalden, A. Piarristeguy, A. Pradel, C. Longeaud, M. Wuttig, Appl. Phys. Lett. 105 (2014) 092108.
[31] J. Luckas, S. Kremers, D. Krebs, M. Salinga, M. Wuttig, C. Longeaud, J. Appl. Phys. 110 (2011) S013719.
[32] J.-W. Park, S.H. Eom, H. Lee, J.L.F.D. Silva, Y.-S. Kang, T.-Y. Lee, Y.H. Khang, Phys. Rev. B 80 (2009) 115209.
[33] B.S. Lee, J.R. Abelson, S.G. Bishop, D.H. Kang, B. K. Cheong, K.B. Kim, J. Appl. Phys. 97 (2005) 093509.

[34] T. Kato, K. Tanaka, Jpn. J. Appl. Phys. 144 (2005) 7340.
[35] M. Popescu, Non-Crystalline Chalcogenides, Springer, Berlin, 2000.
[36] P. Richet, Geochim. Cosmochim. Acta 48 (1984) 471.
[37] B. Effey, R.L. Cappelletti, Phys. Rev. B 59 (1999) 4119.
[38] N. Mousseau, D.A. Drabold, Eur. Phys. J. B 17 (2000) 667.
[39] M. Micoulaut, G.G. Naumis, Recent research developments in non-crystalline solids, in: S.G. Pandalai (Ed.), Transworld Research Network volume 2, 2002, p. 363.
[40] K. Gunasekera, P. Boolchand, M. Micoulaut, J. Phys. Chem. B 117 (2013) 10027.
[41] P. Jévári, I. Kaban, J. Steiner, B. Beuneu, A. Schöps, M.A. Webb, Phys. Rev. B 77 (2008) 035202.
[42] J. Kalb, M. Wuttig, F. Spaepen, J. Mater. Res. 22 (2007) 748.
[43] J. Orava, L. Greer, B. Gholipour, D.W. Hewak, C.E. Smith, Nat. Mater. 11 (2012) 279.
[44] A.N. Sreeram, D.R. Swiler, A.K. Varshneya, J. Non-Cryst. Solids 127 (1991) 287.
[45] J.H. Gibbs, E.A.D. Marzio, J. Chem. Phys. 28 (1958) 373.
[46] M. Micoulaut, G.G. Naumis, Europhys. Lett. 47 (1999) 568.
[47] G.G. Naumis, Phys. Rev. B 73 (2005) 172202.
[48] P.K. Gupta, J.C. Mauro, J. Chem. Phys. 130 (2009) 094503.
[49] P. Boolchand, D.G. Georgiev, T. Qu, F. Wang, L. Cai, S. Chakravarty, Comptes-Rendus Chimie 5 (2002) 713.
[50] P. Boolchand, W.J. Bresser, Philos. Mag. B 80 (2000) 1757.
[51] J.H. Lee, J.H. Yi, W.H. Lee, Y.G. Choi, J. Non-Cryst. Solids 456 (2017) 27.
[52] J.K. Olson, H. Li, P.C. Taylor, J. Ovonic Res. 1 (2005) 1.
[53] O. Kostadinova, S. N. Yannopoulos, J. Non-Cryst. solids 355 (2009) 2040.
[54] M.B. Myers, J.S. Berkes, J. Non-Cryst. Solids 8-10 (1972) 804.
[55] D. Tonchev, S.O. Kasap, J. Non-Cryst. Solids 248 (1999) 28.
[56] E. Morales-Sanchez, E.F. Prokhorov, A. Mendoza-Galvan, J. Gonzalez-Hernandez, J. Appl. Phys. 91 (2002) 697.
[57] J. Kalb, F. Spaepen, M. Wuttig, Appl. Phys. Lett. 84 (2004) 5240.
[58] J.-Y. Cho, D. Kim, Y.-J. Park, T.-Y. Yang, Y.-Y. Lee, Y.C. Joo, Acta Mater. 94 (2015) 143.
[59] A. Sebastian, M.L. Gallo, D. Krebs, Nat. Commun. 5 (2014) 4314.
[60] B. Chen, G.H.t. Brink, G. Plasantzas, B.J. Kooi, J. Phys. Chem. C 121 (2017) 8569.
[61] R. Inoue, T. Kanaya, T. Yamada, K. Shibata, K. Fukao, Phys. Rev. E 97 (2018) 012501.
[62] J.C. Phillips, J. Non-Cryst. Solids1979, 34, 153.
[63] M.F. Thorpe, J. Non-Cryst. Solids, 1983, 57355.
[64] K. Gunasekara, S. Bhosle, P. Boolchand, M. Micoulaut, J. Chem. Phys. 139 (2013) 164511.
[65] M. Bauchy, M. Micoulaut, Nat. Commun. 6 (2015) 6398.
[66] R. Azoulay, H. Thibierge, A. Brenac, J. Non-Cryst. Solids 18 (1978) 33.
[67] M. Micoulaut, Am. Miner. 93 (2008) 1732.
[68] M. Micoulaut, Adv. Phys. X 1 (2016) 147.
[69] K.P. Lakshmi, S. Asokan, J. Non-Cryst. Solids 377 (2013) 175.
[70] K. Gunasekera, P. Boolchand, M. Micoulaut, J. Appl. Phys. 115 (2014) 164905.
[71] A. Chaturvedi, G.S. Varma, S. Asokan, U. Ramamurty, J. Non-Cryst. Solids, 2020, 543120112.
[72] M. Micoulaut, C. Otjacques, J.-Y. Raty, C. Bichara, Phys. Rev. B 81 (2010) 174206.
[73] M. Micoulaut, H. Flores-Ruiz, Unpublished.
[74] M. Anbarasu, S. Asokan, J. Phys. D 40 (2007) 7515.
[75] Z. Yang, P. Lucas, J. Am. Ceram. Soc. 92 (2009) 2920.
[76] C.N. Murthy, V. Ganesan, S. Asokan, Appl. Phys. A 81 (2005) 939.
[77] D. Roy, B. Tanujit, K.B. Jagannatha, G. Sreevidya Varma, S. Asokan, C. Das, J. Non-Cryst. Solids 531 (2020) 119863.